ELSEVIER

Journal of Structural Geology 27 (2005) 1061–1068

JOURNAL OF STRUCTURAL GEOLOGY

www.elsevier.com/locate/jsg

Coeval folding and boudinage in four dimensions

Janet Zulauf*, Gernold Zulauf

Department of Geology and Palaeontology, University of Frankfurt a.M., Senckenberganlage 32-34, D-60054 Frankfurt, Germany

Received 23 September 2004; received in revised form 25 March 2005; accepted 1 April 2005

Abstract

Scaled analogue experiments have been carried out incrementally to demonstrate the growth of constrictional folds and boudins through space and time. Pure constriction acted on a single stiff layer that was embedded in a weak matrix, with the layer trending parallel to the *X*-axis of the constrictional strain ellipsoid. The viscosity ratio between non-linear viscous layer and matrix was set at ca. 13. Three-dimensional images of the incrementally deformed layer have been obtained using computer tomography. They yielded clear evidence that D_1-folds and D_1-boudins show striking interactions when growing *simultaneously* at low to moderate finite strain. The axes of D_1-folds are subparallel and the axes of D_1-boudins are subperpendicular to the *X*-axis of the constrictional strain ellipsoid. The normalized wavelengths of D_1-folds and D_1-boudins, and the amplitudes of D_1-folds, are fixed already at low finite strain (-5%) and do not significantly change as deformation proceeds. The normalized wavelength of both structures is not so in line as suggested by theoretical studies. At higher degrees of finite strain, D_1-boudins are affected by D_2-folds, and rotated limbs of the latter show D_2-boudinage, resulting in complex deformation patterns that are difficult to identify in the field. The model results are important for the analysis and interpretation of deformation structures in rheologically stratified rocks undergoing dislocation creep under bulk constriction. Tectonic settings where constrictional folds and boudins may develop simultaneously are stems of salt diapirs, subduction zones or thermal plumes.

Keywords: Constriction; Analogue modelling; Diapir; Folding; Boudinage

1. Introduction

Buckle folds and boudins are common structures in rheologically stratified rocks and their geometry is widely used to constrain the kinematics, strain and rheology of natural tectonites (e.g. Ramberg, 1955; Sherwin and Chapple, 1968; Cobbold, 1976; Hudleston, 1973, 1986; Fletcher and Sherwin, 1978; Hudleston and Holst, 1984; Lacassin et al., 1993; Lan and Hudleston, 1996; Goscombe et al., 2004). In classical textbooks (e.g. Ramsay and Huber, 1987; Price and Cosgrove, 1990; Twiss and Moores, 1992; Gosh, 1993; Davis and Reynolds, 1996; Van der Pluijm and Marshak, 1997) buckle folds and boudins are largely treated as separate, 2D structures that result from plane-strain deformation of one or more stiff layers embedded in a weak matrix, with the layer oriented perpendicular to the *X*- and *Y*-axis of the finite strain ellipsoid, respectively. Consequently, folds and boudins should not develop simultaneously.

Results of theoretical studies (Ramberg, 1959, fig. 7; Ramsay, 1967; Talbot and Sokoutis, 1995; Weijermars, 1997, fig. 14.24) and analogue scale-model experiments (Kobberger and Zulauf, 1995; Zulauf et al., 2003), on the other hand, suggest that folds and boudins may grow during one single deformation event. This holds for all types of bulk coaxial deformation geometry (from pure flattening via plane strain to pure constriction), if particular geometrical and rheological boundary conditions are given. However, as the results of previous 3D-studies are based only on finite deformation structures, they cannot be used to prove if both structures grew simultaneously or in sequence.

The aim of the present work is to extend the earlier experimental studies of Kobberger and Zulauf (1995) and Zulauf et al. (2003). Different types of plasticine have been used for a stiff layer and a weaker matrix to model folding and boudinaging in rocks with power-law rheology. Layer and matrix underwent pure constriction, with the initially

* Corresponding author. Tel.: +49 69 79822108; fax: +49 069 79822958.

E-mail address: j.zulauf@em.uni-frankfurt.de (J. Zulauf).

0191-8141/$ - see front matter © 2005 Elsevier Ltd. All rights reserved.
doi:10.1016/j.jsg.2005.04.003

Table 1
Geometrical data of D_1-folds and D_1-boudins at 40% finite strain

	Run	I	II	III
	Number of deformation breaks	0	3	7
	ΔH (%)	11±19	19±13	0±11
D_1-boudins	N	21±3	17±3	17±4
	W_a (mm)	8.9	13.4	12.3
	W_d	5.0±2.8	6.1±3.4	6.5±4.2
D_1-folds	N	4±1	2±1	2±1
	W_a (mm)	17.0	16.9	29.7
	W_d	9.6±3.0	9.9±2.9	15.6±4.7
	A (mm)	1.1±0.6	0.8±0.5	0.9±0.5

A, amplitude of folds; ΔH, change in layer thickness; N, number of instabilities; W_a, dominant wavelength of instabilities; W_d, normalized dominant wavelength of instabilities.

planar layer oriented parallel to the X-axis of the finite strain ellipsoid. The deformation geometry of the layer has been analysed step by step using computer tomography (CT). A major advantage of this procedure is that the 3D-geometry of the developing 3D-deformation structures can be continually observed to finite amplitudes. It will be shown that (1) folds and boudins grow simultaneously during one and the same deformation event, (2) both structures do mutually interact, and (3) at least two generations of folds and boudins develop as deformation proceeds to higher finite strains. The results are important for the analysis and interpretation of deformation structures in rheologically stratified rocks undergoing dislocation creep under bulk constriction. Examples for constrictional tectonites are curtain folds in the stems of salt diapirs (Talbot and Jackson, 1987) and folds/boudins of subduction zones (Zulauf, 1997; Zulauf et al., 2002).

2. Methods, material and apparatus

The deformation apparatus used for the constrictional experiments consists of six aluminium plates which have been orthogonally assembled on top of a basal PVC plate. The movement of the plates allows pure constrictional strain to be performed (for further details on the machine, see Zulauf et al. (2003)). To reduce boundary effects due to friction between the specimen and the aluminium plates, the sides of the specimen were lubricated with vaseline. The initial model dimensions are 15×15×15 cm. The analogue material consists of plasticine, a strain-rate softening material, the rheological parameters of which have been determined by previous investigations (for details concerning composition, rheological properties and supplier, see Zulauf and Zulauf (2004)). The experiments have been carried out at a temperature T of 25 °C with a viscosity contrast m of 13 between the stiff layer (Kolb brown plasticine) and the weak matrix (Beck's orange plasticine with 125 ml oil kg^{-1}). The apparent viscosity η and stress exponent n for the layer are 7.2×10^8 Pa s and 5.8, respectively, and for the matrix 6.1×10^7 Pa s and 7.0, respectively. These values are valid for a finite strain $e_{Y=Z}$ of 10% and a strain rate $\dot{e}$ of 6×10^{-5} s^{-1}. The matrix flows in steady state. The layer shows weak strain hardening (for further details, see Zulauf and Zulauf (2004)).

Three different experimental runs have been carried out to show the impact of stress relaxation due to deformation interruption. The first run was carried out without interruption. During the second and third runs, the deformation was stopped in each case at strain increments of 10 and 5%, respectively. The finite strain rate $\dot{e}$ was ca. 6×10^{-5} s^{-1}. Every experiment was finished at a finite strain of

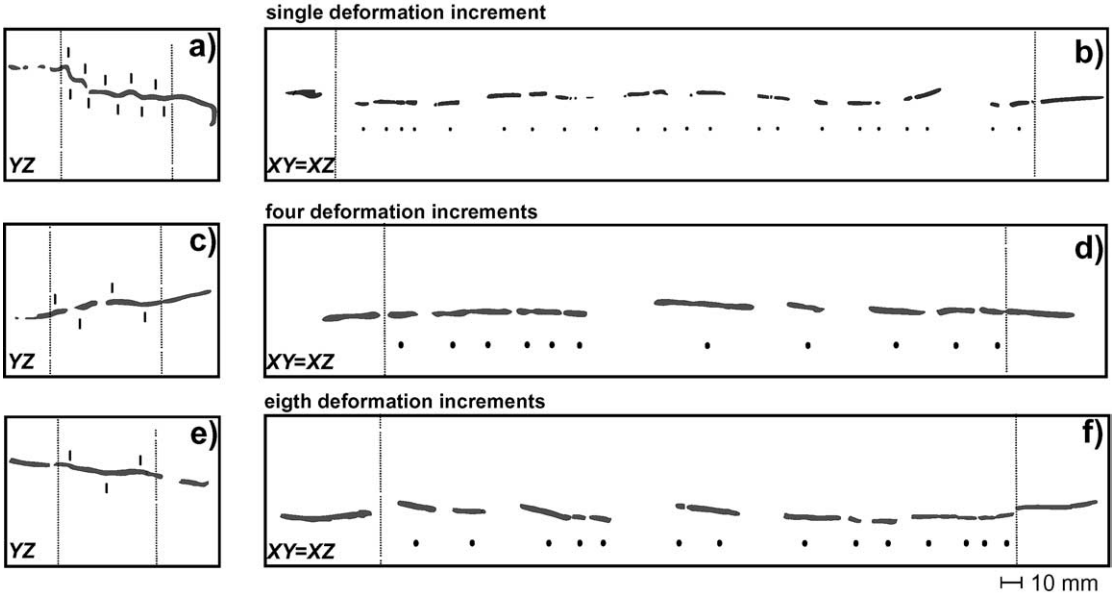

Fig. 1. Y- and $XY{=}XZ$-sections of different runs showing the geometry of the stiff layer after −40% finite strain. (a) and (b) Run 1 (single deformation increment); (c) and (d) Run 2 (four deformation increments); (e) and (f) Run 3 (eight deformation increments); vertical dashed lines indicate the boundaries of evaluated domain; point and dash indicate the number of structures (for further explanation, see text).

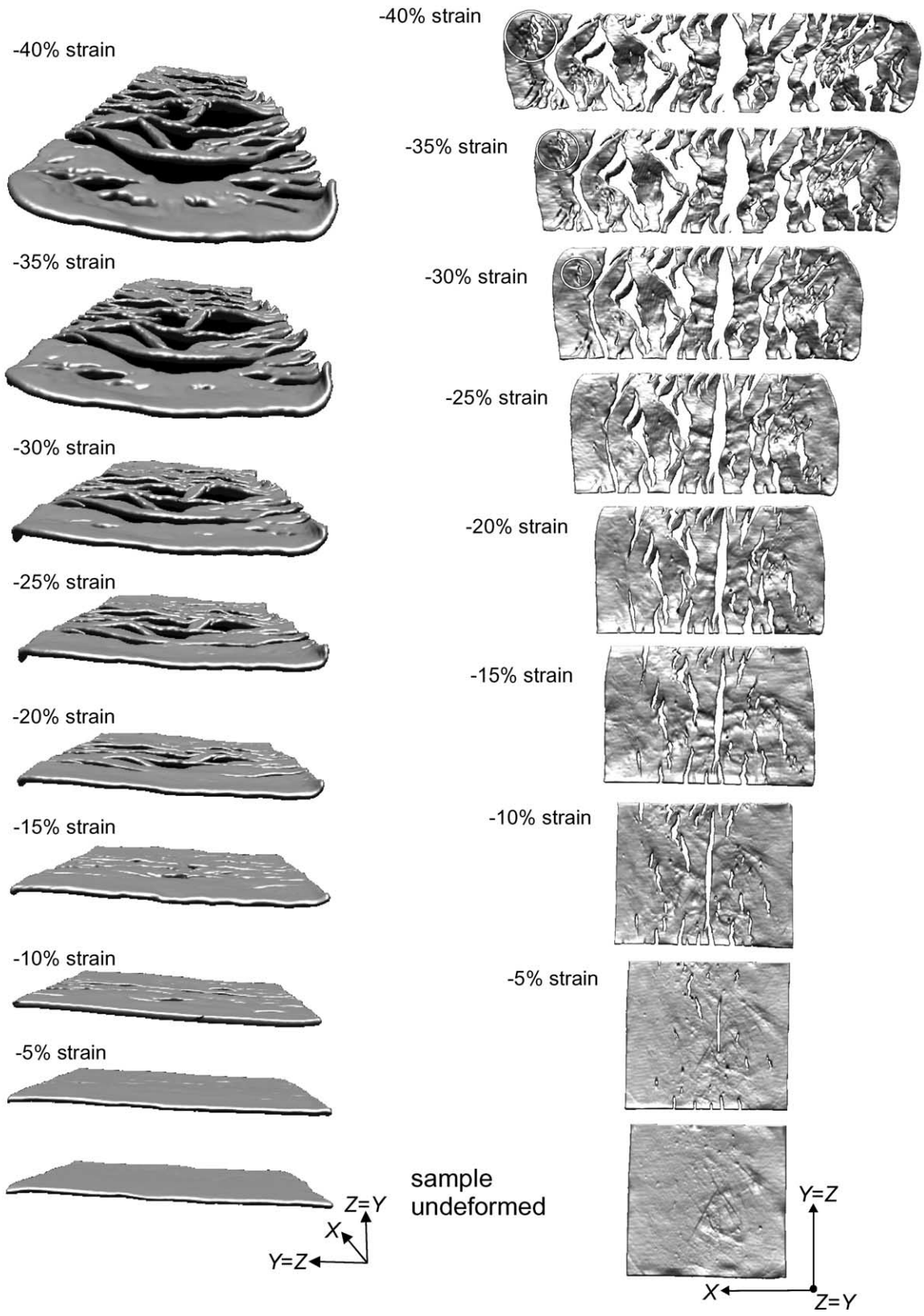

Fig. 2. Three-dimensional views of stiff layer, based on computer tomography, showing the development of constrictional folds and boudins at different deformation states of Run 3. The left column in particular shows the development of D_1-folds in views slightly oblique to the *X*-axis of the finite strain ellipsoid. The right column shows the growth of D_1-boudins and—at progressive strain states—the development of D_2-folds and D_2-boudins in views perpendicular to the layer. White circles show drawn boudins (for further explanation see text and Fig. 5).

$e_{Y=Z} = -40\%$. The initial thickness of the stiff layer H_i was 1.7 ± 0.2 mm. After having imposed the respective incremental strain, the sample was removed from the apparatus and analysed using computer tomography (CT). The CT-studies were performed on a multislice spiral CT-scanner (Somatom Plus 4, Volume Zoom, Siemens Erlangen). In order to visualize the deformation structure using CT, a sufficient contrast in density between layer and matrix is required. According to details reported by the manufacturer and X-ray diffraction analyses, Kolb brown plasticine of the stiff layer contains barite as filler material, whereas Beck's orange plasticine includes potato starch. As a result, the X-ray contrast was sufficient to distinguish layer and matrix in CT images. Geometrical parameters of folds and boudins have been determined from CT-images using the program Open QVis (Rezk-Salama, 2002).

Apart from CT images, the samples with a finite strain of -40% have further been investigated using conventional cuts along *YZ* and $XY = XZ$, the latter being obtained using a wire saw (for details, see Zulauf et al. (2003)).

The initial wavelength of the folds (W_i; sensu Ramsay and Huber, 1987, p. 383) has been determined by measuring the average fold arc lengths W_a (Sherwin and Chapple, 1968; Hudleston, 1973; Fletcher and Sherwin, 1978). The normalized initial wavelength W_d is calculated by dividing the initial wavelength through the finite layer thickness H_f. Because of boundary effects, geometrical parameters have not been determined from folds and boudins of the marginal parts of the deformed samples.

3. Results

When comparing the final deformation states of the three runs, a difference in deformation geometry of the stiff layer is obvious from the conventional cuts (Fig. 1). There are folds and few boudins in *YZ*-sections and boudins in $XY = XZ$-sections. As these structures are succeeded by a second generation of boudins and folds, as is visible in CT-images (see below), they are referred to as D_1-folds and D_1-boudins. The structures are more mature (concerning N, W_d and A, see Table 1) in experiments in which deformation was continuous compared with those experiments that have been interrupted for screening and thus could multiply relax (Fig. 1a and b). Nevertheless, when taking into account the uncertainties, the number and the wavelength of boudins is the same throughout the different runs (Table 1). The same holds for the number, amplitude and normalized dominant wavelength of folds. Moreover, the thickness of the stiff layer did not significantly change during deformation.

The change in deformation geometry of the stiff layer at prescribed strain increments is obvious only from CT images. Both D_1-folds and D_1-boudins develop already at very low strain magnitudes ($e_{Y=Z} = -5$ to -10%; Fig. 2). The axes of initial D_1-folds are trending subparallel and the long axes of initial D_1-boudins are trending subperpendicular to the *X*-axis of the finite strain ellipsoid (Figs. 2 and 3). Most of the necks are discontinuous. This holds particularly for low-strain stages. With progressive strain, existing necks show widening and additional necks occur (Fig. 2). The number of D_1-boudins increases almost linearly as deformation proceeds (Fig. 4a), whereas the wavelength is fixed at ca. -5% strain and does not significantly change within uncertainty at higher strain magnitudes (Fig. 4d). In contrast to the boudins, the number of D_1-folds is almost stable at $< -10\%$ finite strain (Fig. 4a). The same holds for the amplitude and the wavelength

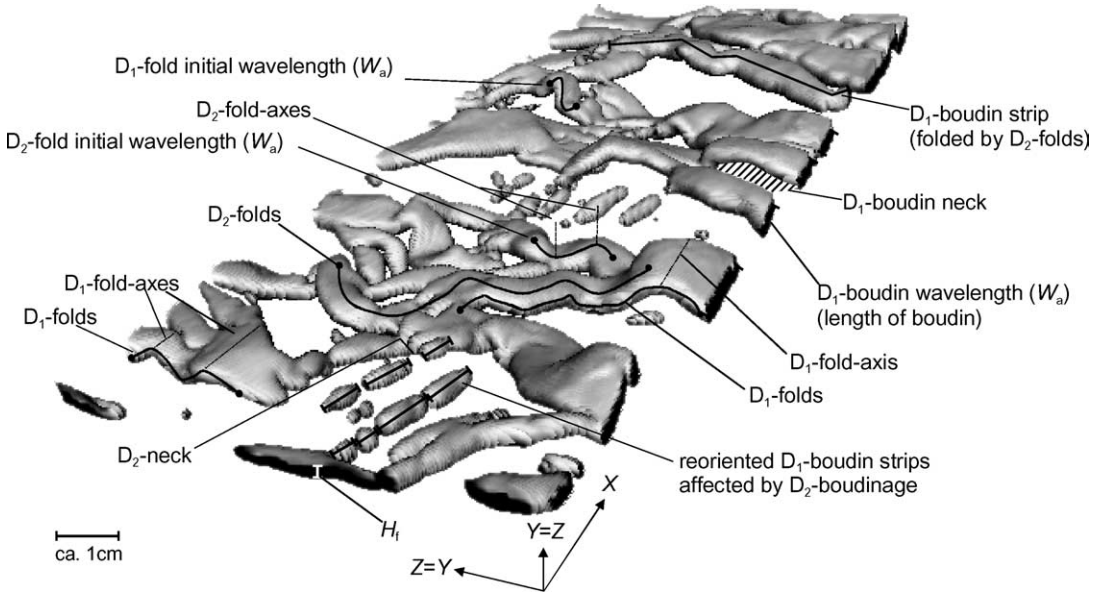

Fig. 3. CT-image showing the complex deformation geometry of the layer at $e_{Y=Z} = -40\%$. Individual structural elements are indicated. Sample with the same viscosity contrast as in Fig. 2 but a single deformation increment.

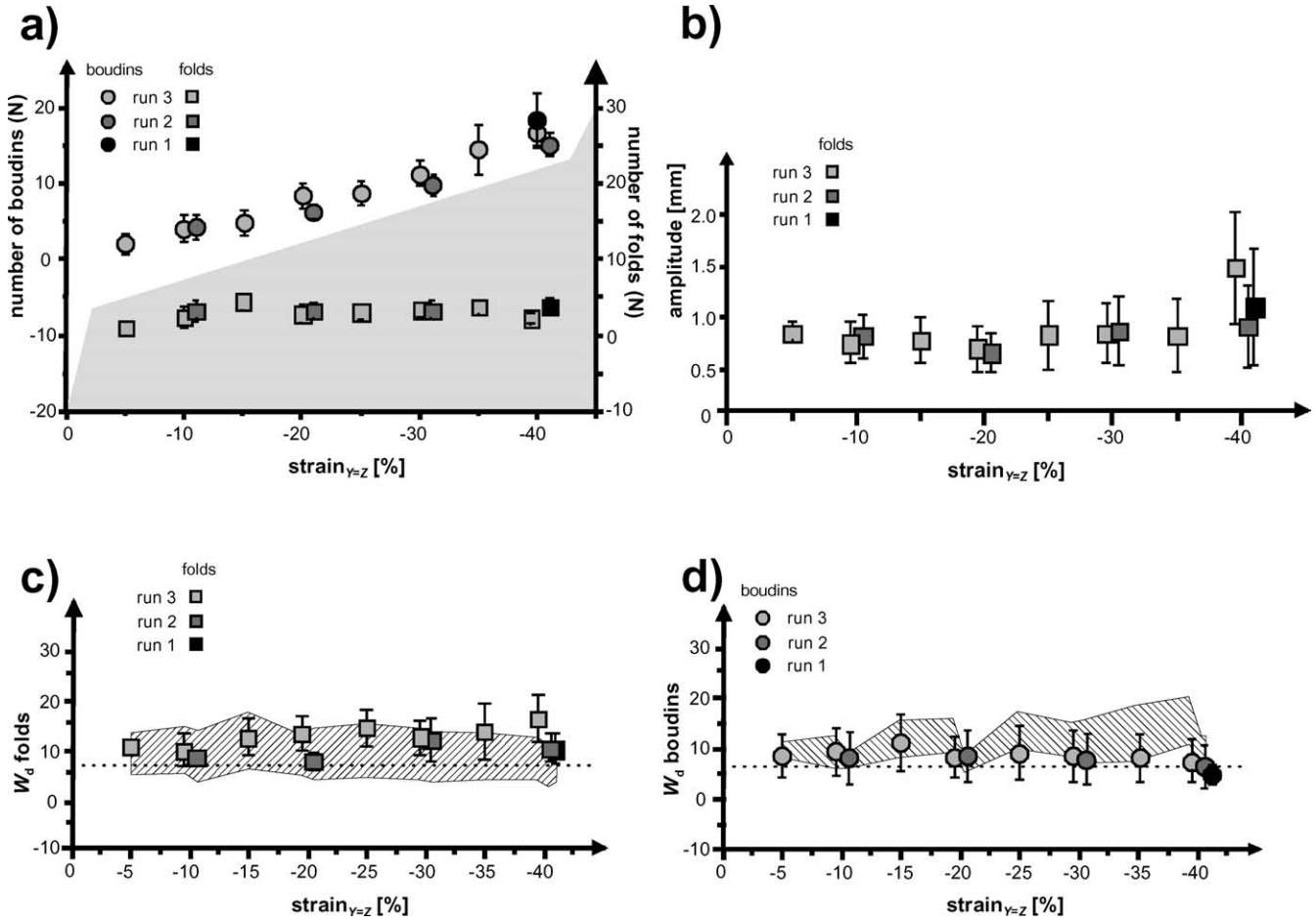

Fig. 4. Geometrical parameters of D_1-folds and D_1-boudins at increasing strain. To improve readability, data points have been slightly laterally shifted. (a) Number of D_1-boudins and D_1-folds versus finite strain. (b) Amplitude of D_1-folds versus finite strain. (c) Normalized dominant wavelength of D_1-folds versus finite strain (shaded area indicates values of D_2-boudins). (d) Normalized dominant wavelength of D_1-boudins versus finite strain (shaded area indicates values of D_1-folds). Horizontal dashed lines in (c) and (d) indicate theoretical normalized wavelength calculated using Eq. (1).

(arc length) of D_1-folds when considering the uncertainties (Fig. 4b and c).

At −20 to −30% finite strain, additional structures develop. D_1-boudins are folded by D_2-folds, the latter with axes trending subperpendicular to the layer (Figs. 2 and 3). Moreover, those D_1-boudins that have been rotated and are aligned subparallel to the *X*-axis underwent additional boudinaging, resulting in D_2-boudins (which are well documented in Fig. 3).

4. Discussion

Because the final deformation geometry of run 1 (uninterrupted deformation) is very similar to that of runs 2 and 3 (interrupted deformation), the stress relaxation due to the break in deformation is of minor importance and the results obtained from the incremental runs can be used to assess general growth characteristics of constrictional folds and boudins. If we try to apply these characteristics to natural rocks, the models should be properly scaled, meaning that geometrical, kinematical and dynamical similarity between model and natural tectonite are required (Hubbert, 1937; Ramberg, 1981; Weijermars and Schmeling, 1986). Dynamic similarity is given in the present case, as natural rocks undergoing dislocation creep and the non-linear viscous plasticine are geometrically and rheologically similar. Constrictional folds and boudins may occur on every scale and the stress–strain curves of model and natural tectonite have similar shapes and differ only in the scaling of the stress axis.

The CT analyses have been used to carry out spatio-temporal analyses of the incrementally deformed samples. They confirm previous assumptions (Kobberger and Zulauf, 1995; Zulauf et al., 2003) that both D_1-folds and -boudins do actually grow simultaneously under pure constriction if a stiff layer is embedded in a weaker matrix, with the layer being oriented parallel to the *X*-axis of the finite strain ellipsoid. The observation that the dominant wavelength of D_1-folds and -boudins is fixed already during early

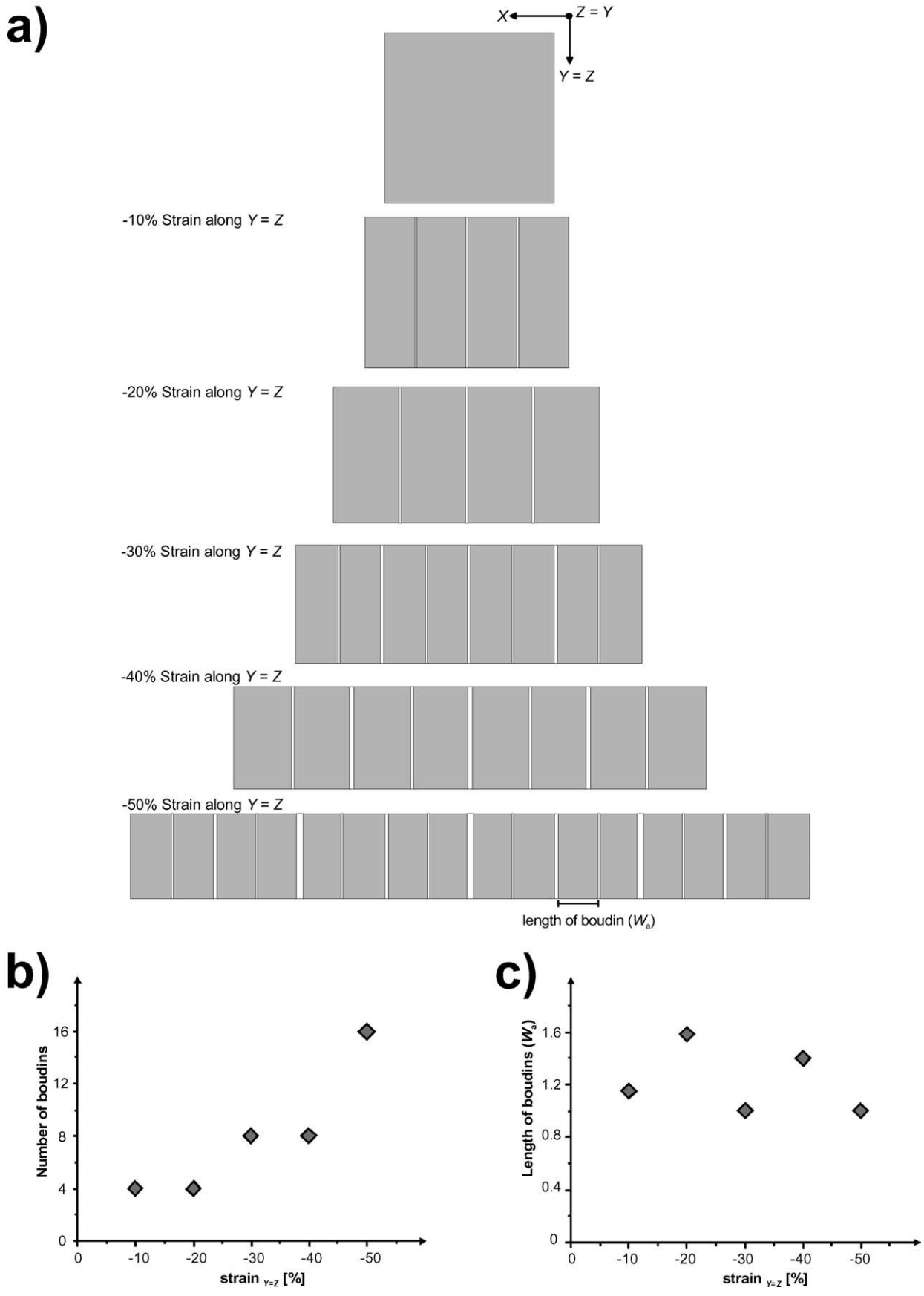

Fig. 5. (a) Schematic drawing of the development of constrictional D_1-boudins. (b) Number of boudins versus finite strain. (c) Length of boudins versus finite strain.

deformation stages is in line with results from previous analogue modelling based on bulk plane strain (e.g. Chapple, 1968; Hudleston, 1973). Theories of buckle folding in non-linear materials suggest the initial wavelength of buckle folds and boudins to be the same. The geometrical and rheological parameters of these instabilities are related by the following equation (Fletcher, 1974; Smith, 1977, 1979):

$$L_d \approx 3.46(n_2^{1/6}/n_1^{1/3})(\eta_1/\eta_2)^{1/3} \quad (1)$$

where L_d is the theoretical wavelength/finite thickness, and n_1, η_1 and n_2, η_2 are the stress exponents and the effective viscosities in the flow laws for layer and matrix, respectively.

To compare the theoretical value (L_d) with the average wavelength (W_a) measured in the experiments, we normalized the initial wavelength of the structures with the following equation:

$$W_d = W_a/H_f \quad (2)$$

where W_d is the normalized dominant wavelength, W_a is the average initial wavelength and H_f is the finite thickness.

From the rheological parameters of the plasticine used, L_d is calculated at 6.3. This value is similar to the normalized wavelength of the D_1-boudins ($W_d = 5.0 \pm 2.8$, 6.1 ± 3.4, 6.5 ± 4.2), the latter showing relatively large uncertainties (Fig. 4d). The normalized initial wavelengths of the D_1-folds ($W_d = 9.6 \pm 3.0$, 9.9 ± 2.9, 15.6 ± 4.7), however, clearly exceed the L_d-value, even if uncertainties are considered (Fig. 4c).

An unexpected result of the experiments is the fact that the amplitude of the D_1-folds is fixed already at low strain magnitudes and does not significantly change with progressive deformation until high magnitudes of strain are achieved (Fig. 4b). For example, the amplitude of plane strain folds grows with progressive strain (Hudleston, 1973). The constant amplitude of constrictional D_1-folds can be regarded to be a diagnostic feature for buckling in constrictional environments. A further characteristic feature is that layer thickness does not markedly change with progressive strain (cf. Kobberger and Zulauf, 1995; Zulauf et al., 2003). All these features can be used to distinguish the constrictional structures of the present study from coeval folds and boudins that result from bulk plane and flattening strain (Zulauf et al., 2003).

A further unexpected feature of the experiments is that with progressive strain the number of boudins increases, while the wavelength of boudins is almost fixed already at low finite strain. The increasing number of boudins are closely related to the formation of new necks as deformation proceeds (Ramberg, 1955). The formation of these additional necks is possible as the wavelength of boudins increases with progressive strain, meaning that pre-existing boudins are drawn boudins (Goscombe et al., 2004) which were ductilely stretched after coming into being (Fig. 5). As the thickness of the stiff layer does not significantly change throughout the experiment, the increase in boudin wavelength supports shear stresses to work more effectively along the boudin/matrix interface, leading to enhanced tensile stresses within the boudin. If the length of the boudin exceeds a critical value, its tensile strength will be exceeded and a new neck will form in the central part of the boudin (Ramberg, 1955). Thus, the wavelength of the D_1-boudins is only approximately constant. It varies within a distinct interval, which is indicated by the uncertainties depicted in Fig. 4d. The almost constant value of the wavelength of D_1-boudins probably reflects a steady state that includes formation, widening and destruction (necking) of boudins, whereas the thickness of boudins does not significantly change.

As is obvious from the CT images, the interaction between D_1-folds and D_1-boudins partly results in initial oblique orientation of the boudins and necks with respect to the principal strain axes. If bulk strain increases, the geometry of the layer becomes more and more complex. Progressive shortening parallel to the long axis of the D_1-boudins led to the development of D_2-folds (Figs. 3 and 6). The D_1-boudin strips were superposed by the D_2-folding and thus show a more or less oblique position with respect to the principal strain axes. As D_2-folding proceeds, some of

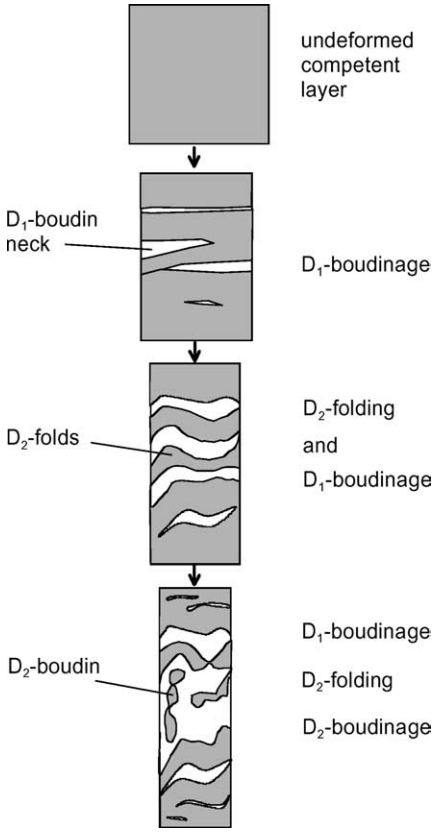

Fig. 6. Schematic line drawing showing the development of different types of folds and boudins at increasing constrictional strain in a section that is oriented parallel to the stiff layer. Note that D_1-folds do not appear in these sections.

the D_1-boudins rotate progressively towards the *X*-axis of the finite strain ellipsoid. If the rotation is sufficient for the D_1-boudin strips to become subparallel to the *X*-axis, the D_1-boudins are in the orientation where they may develop D_2-necks. Thus, at high strain magnitudes pure constriction causes a complex deformation pattern if a stiff layer is embedded in a weak matrix with the D_1-boudin strips trending parallel to the *X*-axis. In cases of rock analogues, the analysis of these three-dimensional structures is possible using CT-images. In natural environments, however, the structures produced in the present study can be identified only in those cases where rocks are well exposed in three dimensions.

Acknowledgements

We are grateful to B. Tomandl and P. Hastreiter for support when making CT images. We further acknowledge the help with the visualization of CT images by C. Rezk-Salma and M. Bauer (Computer Graphics Group at Technical Faculty at the University of Erlangen). Many thanks also to B.D. Goscombe and C.J. Talbot for their constructive reviews. This study was supported by Deutsche Forschungsgemeinschaft [Zu 73/7-2] which is gratefully acknowledged.

References

Chapple, W.M., 1968. A mathematical theory of finite-amplitude rock-folding. Geological Society of America Bulletin 79, 47–68.

Cobbold, P.R., 1976. Fold shapes as functions of progressive strain. Philosphical Transactions; Royal Society London Series A 283, 129–138.

Davis, G.H., Reynolds, S.J., 1996. Structural Geology of Rocks and Regions. Wiley, New York.

Fletcher, R.C., 1974. Wavelength selection in the folding of a single layer with power-law rheology. American Journal of Science 274, 1029–1043.

Fletcher, R.C., Sherwin, J., 1978. Arc lengths of single fold layers: a discussion of the comparison between theory and observation. American Journal of Science 278, 1085–1098.

Goscombe, B.D., Passchier, C.W., Hand, M., 2004. Boudinage classification: end-member boudin types and modified boudin structures. Journal of Structural Geology 26, 739–763.

Gosh, S.K., 1993. Structural Geology. Fundamentals and Modern Developments. Pergamon Press, Oxford.

Hubbert, M.K., 1937. Theory of scale models as applied to the study of geologic structures. Geological Society American Bulletin 48, 1459–1519.

Hudleston, P.J., 1973. An analysis of "single-layer" folds developed experimentally in viscous media. Tectonophysics 16, 189–214.

Hudleston, P.J., 1986. Extracting information from folds in rocks. Journal of Geological Education 34, 237–245.

Hudleston, P.J., Holst, T.B., 1984. Strain analysis and fold shape in a limestone layer and implications for layer rheology. Tectonophysics 106, 321–347.

Kobberger, G., Zulauf, G., 1995. Experimental folding and boudinage under pure constrictional conditions. Journal of Structural Geology 17, 1055–1063.

Lacassin, R., Leloup, P.H., Tapponnier, P., 1993. Bounds on the strain on large Tertiary shear zones of SE Asia from boudinage restoration. Journal of Structural Geology 15, 677–692.

Lan, L., Hudleston, P., 1996. Rock rheology and sharpness of folds in single layers. Journal of Structural Geology 18, 925–931.

Price, N.J., Cosgrove, J.W., 1990. Analysis of Geological Structures. Press Syndicate of the University of Cambridge, New York.

Ramberg, H., 1955. Natural and experimental boudinage and pinch-and-swell structures. Journal of Geology 63, 512–526.

Ramberg, H., 1959. Evolution of ptygmatic folding. Norsk Geologisk Tidsskrift 39, 99–152.

Ramberg, H., 1981. Gravity, Deformation and the Earth's Crust. Academic Press, London.

Ramsay, J.G., 1967. Folding and Fracturing of Rocks. McGraw-Hill Book Co, New York.

Ramsay, J.G., Huber, I.H., 1987. The Techniques of Modem Structural Geology, Folds and Fractures, vol. 2. Academic Press, London.

Rezk-Salama, C., 2002. Volume Rendering Techniques for General Purpose Graphics Hardware. Arbeitsberichte des Institutes für Informatik. Friedrich Alexander-Universität Erlangen-Nürnberg, Technische Fakultät, Institut für Informatik, Erlangen.

Sherwin, J.-A., Chapple, W.M., 1968. Wavelengths of single layer folds. A comparison between theory and observation. American Journal of Science 266, 167–178.

Smith, R.B., 1977. Formation of folds, boudinage, and mullions in non-Newtonian materials. Geological Society of America Bulletin 88, 312–320.

Smith, R.B., 1979. The folding of a strongly non-Newtonian layer. American Journal of Science 279, 272–287.

Talbot, C.J., Jackson, M.P.A., 1987. Internal kinematics of salt diapirs. The American Association of Petroleum Geologists Bulletin 71, 1068–1093.

Talbot, C.J., Sokoutis, D., 1995. Strain ellipsoids from incompetent dykes: application to volume loss during mylonitization in the Singö gneiss zone, central Sweden. Journal of Structural Geology 17, 927–948.

Twiss, R.J., Moores, E.M., 1992. Structural Geology. W.H. Freeman and Company, New York.

Van der Pluijm, B.A., Marshak, S., 1997. Earth Structure. An Introduction to Structural Geology and Tectonics. McGraw-Hill, New York.

Weijermars, R., 1997. Principles of Rock Mechanics. Alboran Science Publishing, Amsterdam.

Weijermars, R., Schmeling, H., 1986. Scaling of Newtonian and non-Newtonian fluid dynamics without inertia for quantitative modeling of rock flow due to gravity (including the concept of rheological similarity). Physics of the Earth and Planetary Interiors 43, 316–330.

Zulauf, G., 1997. Constriction due to subduction: evidence for slab pull in the Mariánské Lázně complex (central European Variscides). Terra Nova 9, 232–236.

Zulauf, J., Zulauf, G., 2004. Rheology of plasticine used as rock analogue: the impact of temperature, composition and strain. Journal of Structural Geology 26, 725–737.

Zulauf, G., Kowalczyk, G., Krahl, J., Petschik, R., Schwanz, S., 2002. The tectonometamorphic evolution of high-pressure low-temperature metamorphic rocks of eastern Crete, Greece: constraints from micro fabrics, strain, illite crystallinity and paleodifferential stress. Journal of Structural Geology 24, 1805–1828.

Zulauf, G., Zulauf, J., Hastreiter, P., Tomandl, B., 2003. A deformation apparatus for three-dimensional coaxial deformation and its application to rheologically stratified analogue material. Journal of Structural Geology 25, 469–480.